Large Amplitude Torsions in Nitrotoluene Isomers Studied by Rotational Spectroscopy and Quantum Chemistry Calculations

Anthony Roucou, Manuel Goubet, Isabelle Kleiner, Sabath Bteich, Arnaud Cuisset

To cite this version:

Anthony Roucou, Manuel Goubet, Isabelle Kleiner, Sabath Bteich, Arnaud Cuisset. Large Amplitude Torsions in Nitrotoluene Isomers Studied by Rotational Spectroscopy and Quantum Chemistry Calculations. ChemPhysChem, 2020, 21 (22), pp.2523-2538. ⟨10.1002/cphc.202000591⟩. ⟨hal-04568655⟩

"Large Amplitude Torsions in Nitrotoluene Isomers Studied by Rotational Spectroscopy and Quantum Chemistry Calculations"

Roucou, Anthony ; Goubet, Manuel ; Kleiner, Isabelle ; Bteich, Sabath ; Cuisset, Arnaud

ABSTRACT

Rotational spectra of ortho-nitrotoluene (2-NT) and para-nitrotoluene(4-NT) have been recorded at low and room temperatures using a supersonic jet Fourier Transform microwave (MW) spectrometer and a millimeter-wave frequency multiplier chain, respectively. Supported by quantum chemistry calculations,the spectral analysis of pure rotation lines in the vibrational ground state has allowed to characterise the rotational energy, the hyperfine structure due to the 14N nucleus and the internal rotation splittings arising from the methyl group. For 2-NT, an anisotropic internal rotation of coupled ## CH3 and ## NO2 torsional motions was identified by quantum chemistry calculations and discussed from the results of the MW analysis. The study of the internal rotation splittings in the spectra of three NT isomers allowed to characterise the internal rotation potentials of the methyl group and to compare them with other mono-substituted toluene derivatives in order to study the isomeric influence on the internal rotation barrier.

CITE THIS VERSION

Roucou, Anthony ; Goubet, Manuel ; Kleiner, Isabelle ; Bteich, Sabath ; Cuisset, Arnaud. *Large Amplitude Torsions in Nitrotoluene Isomers Studied by Rotational Spectroscopy and Quantum Chemistry Calculations.* In: *ChemPhysChem*, Vol. 22, no.22, p. 1 (2020) http://hdl.handle.net/2078.1/237918 -- DOI : 10.1002/cphc.202000591

ChemPhysChem

Articles
doi.org/10.1002/cphc.202000591

Large Amplitude Torsions in Nitrotoluene Isomers Studied by Rotational Spectroscopy and Quantum Chemistry Calculations

Anthony Roucou,*[a, b] Manuel Goubet,[c] Isabelle Kleiner,[d] Sabath Bteich,[a] and Arnaud Cuisset*[a]

Rotational spectra of ortho-nitrotoluene (2-NT) and para-nitrotoluene (4-NT) have been recorded at low and room temperatures using a supersonic jet Fourier Transform microwave (MW) spectrometer and a millimeter-wave frequency multiplier chain, respectively. Supported by quantum chemistry calculations, the spectral analysis of pure rotation lines in the vibrational ground state has allowed to characterise the rotational energy, the hyperfine structure due to the ^{14}N nucleus and the internal rotation splittings arising from the methyl group. For 2-NT, an anisotropic internal rotation of coupled $-CH_3$ and $-NO_2$ torsional motions was identified by quantum chemistry calculations and discussed from the results of the MW analysis. The study of the internal rotation splittings in the spectra of three NT isomers allowed to characterise the internal rotation potentials of the methyl group and to compare them with other mono-substituted toluene derivatives in order to study the isomeric influence on the internal rotation barrier.

1. Introduction

In recent years, intensive research has been conducted to develop a compact, selective and low-cost explosive vapour sensor with subppm detection limits capable of replacing canine detection, but with no success so far. Although high-resolution rovibrational spectroscopy proved to be a powerful tool for the detection, identification and quantification of gaseous molecular species of atmospheric and astrophysical interest, the optical methods used present a lack of sensitivity or selectivity for detection of low volatility explosive vapours at room temperature. Indeed, the energetic compounds have very low saturation vapour pressures at room temperature, for example: Trinitrotoluene (TNT) is one of the most volatile industrially manufactured explosives with a vapour pressure of only 1.3 mPa at 300 K.[1] The volatility of most other explosives such as cyclo-1,3,5-trimethylene-2,4,6-trinitramine (RDX) or pentaerythritol tetranitrate (PETN) are significantly lower by several orders of magnitude. In 2004, D. S. Moore published a review related to instrumentation for detecting traces of gas-phase explosives.[2] Several techniques have been considered but each of them has specific disadvantages for an unambiguous detection of explosive vapors: (i) the ultra-sensitive photothermal deflection,[3] intracavity (Cavity RingDown Spectroscopy)[4] and photoacoustic infrared (IR) spectroscopy probing intense vibrational transitions[5] allowed to measure the gas-phase IR signatures of TNT and RDX but their selectivity does not allow to unambiguously discriminate the compounds of the same family or the isomers (with widths of vibrational bands 100 to 1000 times wider than that of rotational lines), (ii) Raman spectroscopy has also been used to detect residual explosives in signature samples,[6] but its ability to detect very small solid samples does not allow measurements in the gas phase due to a lack of sensitivity, and (iii) promising results have been obtained in the UV/visible domain by laser photofragmentation[7] or by single-photon ionization[8] but they do not exclude the possibility to fragment the parent molecule. Despite the low vapour pressure of industrially manufactured explosives, more volatile chemical markers are added or naturally present in many explosives[9] and usually used for the detection in the atmosphere by specifically trained dogs. Two types of explosive markers can be considered: those that can detect the presence of a bomb and those that allow the authorities to identify the explosive after a bomb explosion. The explosives taggants initially mentioned in the ICAO convention of 1991[10] are the 2,3-dimethyl-2,3-dinitrobutane (DMNB) which is only used in the US, the Ethylene glycol dinitrate (EGDNT) which is used to mark Semtex and the more volatile ortho-mononitrotoluene (2-NT) and para-mononitrotoluene (4-NT) which are used to mark TNT.[11, 12] Those two last markers are the objects of the present study. A first gas phase spectroscopic study at room temperature has been performed in the far infrared (FIR) region for the three NT isomers where the vibrational cross-sections have been measured and assigned at low resolution ($\Delta\nu = 0.5$ cm^{-1}).[13] The results have

---

[a] Dr. A. Roucou, Dr. S. Bteich, Prof. A. Cuisset
Université du Littoral Côte d'Opale, UR 4493, LPCA, Laboratoire de Physico-Chimie de l'Atmosphère, F-59140 Dunkerque, France
E-mail: anthony.roucou@univ-littoral.fr
arnaud.cuisset@univ-littoral.fr
[b] Dr. A. Roucou
Institut de la Matière Condensée et des Nanosciences (IMCN), Université catholique de Louvain, Chemin du Cyclotron 2, 1348 Louvain-la-Neuve, Belgium
[c] Dr. M. Goubet
Univ. Lille, CNRS, UMR8523 – PhLAM – Physique des Lasers Atomes et Molécules, F-59000 Lille, France
[d] Prof. I. Kleiner
Laboratoire Interuniversitaire des Systèmes Atmosphériques (LISA), CNRS UMR 7583, Université Paris-Est Créteil & Université de Paris, Institut Pierre Simon Laplace (IPSL), 61 avenue du Général de Gaulle, F-94010 Créteil cedex, France

Supporting information for this article is available on the WWW under https://doi.org/cphc.202000591 highlighted the selectivity of gas phase THz/FIR spectroscopy for identification of nitro-aromatic compounds and its ability to discriminate the different isomers of mono-nitrotoluene but it was not possible to resolve at room temperature the rotational structure of the rovibrational FIR bands, even at the maximal resolution of the FTIR instrument (10^{-3} cm^{-1}).[14] Indeed, the density of rovibrational lines is so high that it prevented their individual observation at room temperature, which is mostly explained by low rotational constants, numerous hot bands involving the lowest energy modes and splittings due to large amplitude motions. Considering this study, the resolution of the rovibrational structure of FIR fundamental bands at very low temperature could be studied, but it is out of reach for a majority of semi-volatile molecules yet.[15, 16] The opportunity to probe pure rotational transitions of explosive taggants in the microwave (MW) and millimeter-wave (mm-wave) frequency ranges using electronic sources with exceptional spectral purities has been firstly considered for the meta-mononitrotoluene (3-NT) isomer. In this study, a high complexity was encountered from the experimental and theoretical point of view.[17] From an experimental point of view, the mm-wave experimental instrument has been pushed to its limit of sensitivity and resolution resulting in a weak rotational spectrum with low signal-to-noise ratio (S/N) due to weak room temperature vapour pressure ($P_{vap.}(293K) = 8.55$ Pa[18]) and a high density of lines with many blended lines. Concerning the spectroscopic analysis, a specific effective Hamiltonian taking into account the nuclear quadrupole coupling (NQC) for the hyperfine structure observed in MW frequency range and the large amplitude motion of the methyl group presenting a very low internal rotation barrier ($V_3 = 6.7659(24)$ cm^{-1}) were required to reproduce the spectra at the experimental accuracy. As a consequence, a similar approach has been used in this study to measure and analyze the MW and mm-wave spectra of the two TNT markers, 2-NT ($P_{vap.}(293K) = 12.7$ Pa[18]) and 4-NT ($P_{vap.}(293K) = 3.79$ Pa[18]), to reach a full knowledge of the rotational energy description of the nitrotoluene isomers supported by quantum chemistry calculations, to study the influence of the isomeric form on the internal rotation and NQC and, finally to produce a set of reliable ground state molecular constants and a rotational line list for future in situ detection.

2. Results and Discussion

2.1. Spectra analysis

2.1.1. 4-Nitrotoluene

The analysis of 4-NT follows strictly the steps of the 3-NT analysis.[17] Based on quantum chemistry calculations described in computational methods section and presented in details in Table S1 of supporting information I, the jet-cooled MW spectrum (see section 5.1) has been firstly measured and analysed up to $J'' = 12$ and $K_a'' = 6$ taking into account both the coupling with internal rotation of the methyl group, the NQC and the spin statistics. The A1/A2 and B1/B2 species were preliminary assigned using the SPFIT/SPCAT Pickett's programs[19] (semi-rigid rotor model in the I^r representation of A-reduced Watson's Hamiltonian) and completed with the E1/E2 species arising from internal rotation coupling using Ilyushin's code RAM36hf.[20–23] This code especially developed for the analysis of internal rotation splittings of G_{12} point group molecules including high order internal rotation coupling terms for low internal rotation barriers and NQC terms has been firstly used on nitromethane.[23] According to the permanent dipole vector orientation (see Figure 1), only *a*-type transitions have been observed with a total of 304 individual transitions (83 A1/A2, 74 B1/B2, 78 E1 and 69 E2 species) assigned to 226 blended

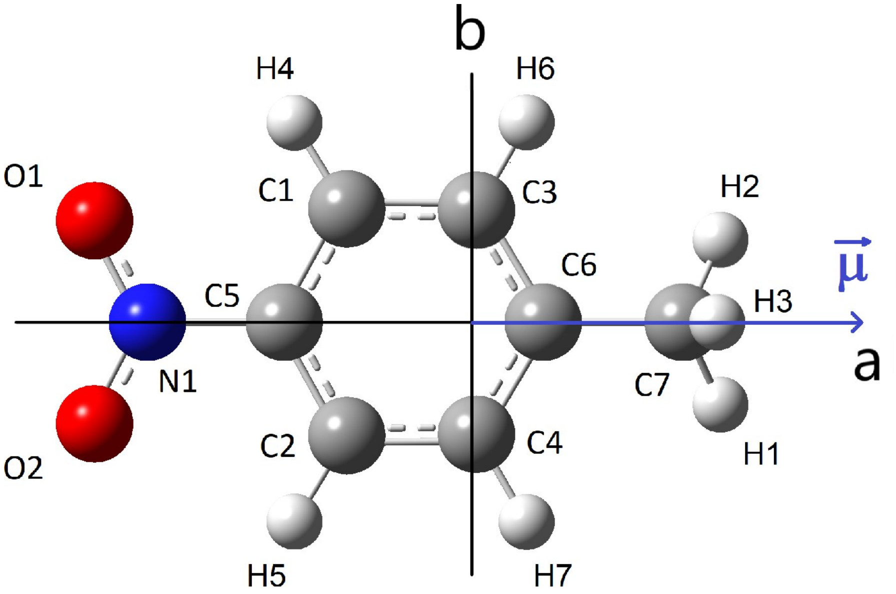

Figure 1. 4-NT geometry optimized at the MP2/cc-pVQZ level of theory in the principal axis orientation. The atoms have been labelled for the spin statistics analysis. All of them are in the (a,b) plane except the hydrogens of the methyl group.

lines with a RMS deviation of 1.97 kHz (1.82 kHz for A1/A2, 2.00 kHz for B1/B2, 1.91 kHz for E1 and 2.16 kHz for E2 species). The E1 and E2 species have been assigned with splittings varying up to 270 MHz. As shown in Figure 2, the hyperfine structures where not all fully resolved.

In order to predict the mm-wave spectra (see section 5.2) by extrapolation, the rotational constants obtained from the fit of the MW lines have been used as initial set of constants for an updated version of RAM36hf adapted for high rotational quantum number values ($J_{max} = 180$). A code has been written to convert the input/output files of RAM36hf in a usable format for the ASCP/SVIEW graphical interface of the AABS Package.[24,25] As shown in zoomed parts of Figure 3, several characteristic features from the ground vibrational state ($v = 0$) may be assigned despite the congestion of the blended lines arising from the internal rotation splittings and the presence of numerous hot band transitions. A total of 3188 transitions (1111 A1/A2, 869 B1/B2, 558 E1 and 650 E2 and species) corresponding to 990 blended lines were fitted up to $J'' = 163$ and $K_a'' = 41$ in a global fit including the MW lines with a total RMS deviation of 105 kHz (96.0 kHz for A1/A2, 101.3 kHz for B1/B2, 116.7 kHz for E1 and 114.4 kHz for E2 species) with a special treatment of

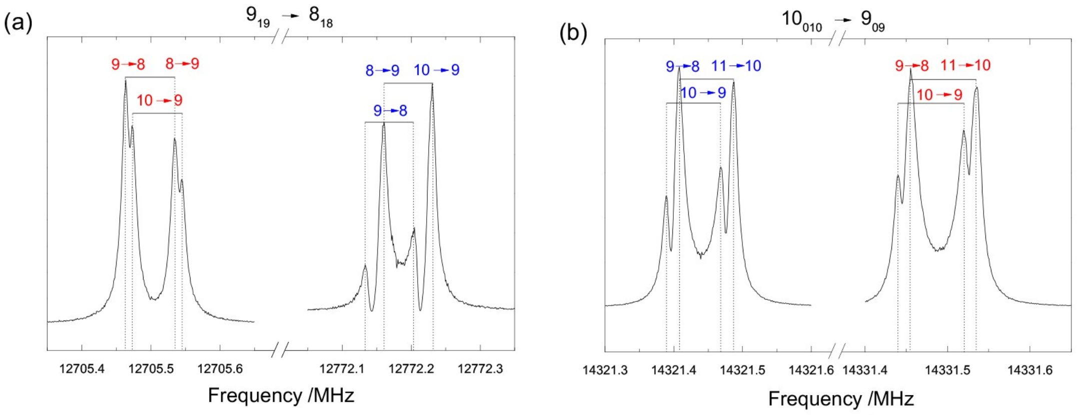

Figure 2. Experimental microwave spectrum of 4-NT for two ^{a}R-type transitions: (a) $9_{1,9}\rightarrow8_{1,8}$ (300 co-added scans) and (b) $10_{0,10}\rightarrow9_{0,9}$ (200 co-added scans). Doppler doublets have been assigned in the F′→F″ format for hyperfine NQC transitions and the internal rotation splitting are identified for the A/B species (in red) and E species (in blue).

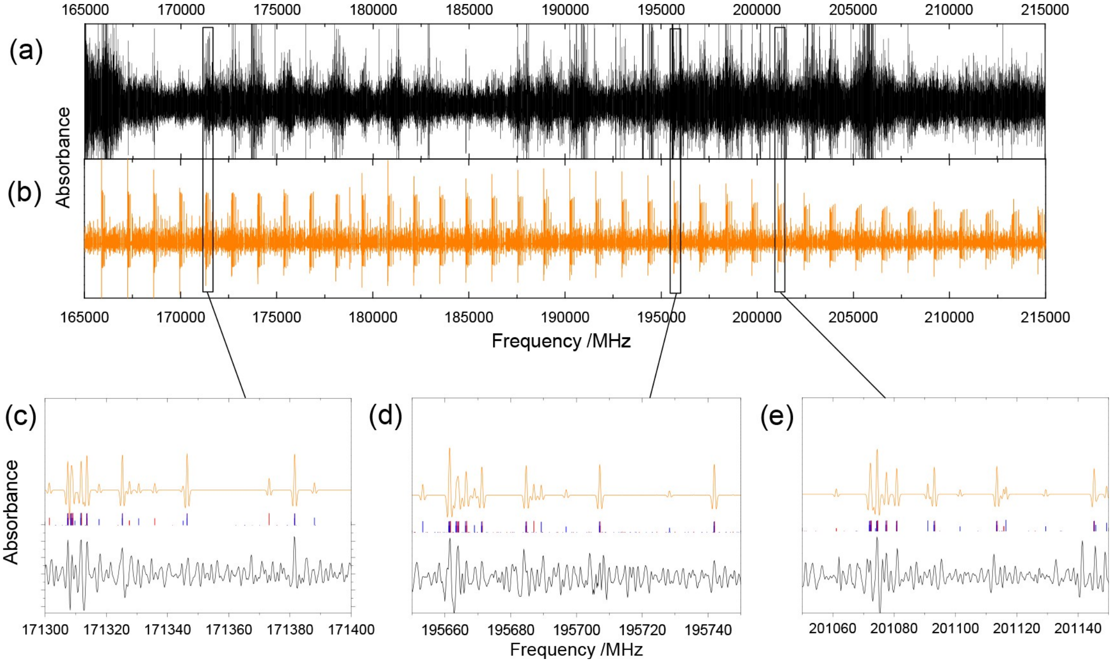

Figure 3. Part of the 70–230 GHz experimental mm-wave spectrum of 4-NT compared to the simulated spectrum obtained from the fit (see section 4.1): (a) is the 165 GH–215 GHz experimental spectrum (black); (b) is the global simulated spectrum for the v = 0 ground state (orange). Some characteristics patterns of 4-NT are presented in (c), (d) and (e) with the individual frequencies calculated from the fit of A/B and E species in red and blue, respectively. All intense saturated spurious patterns in (a) are artefacts of saturated noise due to the sensitivity limit of the spectrometer pushed on its maximum.

blends. Internal rotation splittings have been observed up to several GHz. The molecular constants resulting from the analysis of 4-NT spectra are presented and compared with quantum chemistry calculations in Table 1. The association of mm-wave transitions to MW transitions in the fit provides a better determination of all the molecular constants, in particular the accuracy of Δ_J, Δ_{JK}, δ_J are improved by several orders of magnitude and Δ_K and δ_K have been fitted. Concerning the internal rotation parameters, the accuracy of V_6 is improved by one order of magnitude and the higher order internal rotation coupling parameter F_{bc} is determined. The fitted constants match very well with the calculated values, especially the rotational constants with relative differences lower than 2.3%. NQC and internal rotation barriers are specifically discussed in sections 2.2 and 2.3, respectively.

Table 1. Ground state torsion-rotation constants of the 4-NT obtained from the MW and mm-wave fits of A1/A2, B1/B2, E1 and E2 species with RAM36hf compared with quantum chemistry calculations. Numbers in parentheses represent one standard deviation in units of the least significant digit.

	Unit	RAM36hf MW	RAM36hf MW/mm-wave	Calc.[a]	Operator[b]
A	MHz	3985.927(10)[c]	3985.9141(85)[c]	3894.435	P_a^2
B	MHz	815.376511(82)[c]	815.376644(42)[c]	814.113	P_b^2
C	MHz	677.377020(70)[c]	677.376918(41)[c]	676.603	P_c^2
Δ_J	kHz	0.01188(12)	0.0125519(17)	0.012357	$-P^4$
Δ_{JK}	kHz	0.01295(91)	0.010011(52)	0.009828	$-P^2P_a^2$
Δ_K	kHz	0.321574[f]	0.329(11)	0.321574	$-P_a^4$
δ_J	kHz	0.203(15)	0.00239320(70)	0.002411	$-2P^2\left(P_b^2-P_c^2\right)$
δ_K	kHz	-0.00542[f]	0.05078(18)	-0.00542	$-\left\{P_a^2, \left(P_b^2-P_c^2\right)\right\}$
χ_{aa}	MHz	$-1.1732(56)$	$-1.1724(62)$	-1.3557	$2P_a^2(f(I,J,F)/J(J+1))$
χ_{bb}	MHz	0.258(18)[d]	0.262(19)[d]	0.0387	$2P_b^2(f(I,J,F)/J(J+1))$
χ_{cc}	MHz	0.915(12)	0.910(13)	1.317	$2P_c^2(f(I,J,F)/J(J+1))$
F	cm^{-1}	5.528[f]	5.528[f]	5.528	p_α^2
ρ	unitless	0.0239077(20)[e]	0.0241437(17)[e]	0.024061	$p_\alpha P_a$
V_6	cm^{-1}	12.5(22)	12.22(18)	11.283	$(1/2)(1-cos(6\alpha))$
F_J	kHz	$-1.147(18)$	$-1.146(17)$		$p_\alpha^2P^2$
ρ_J	kHz	0.1586(44)	0.1644(18)		$p_\alpha P_a P^2$
F_{bc}	kHz		0.335(52)		$\left(P_b^2-P_c^2\right)p_\alpha^2$
δ[g]	rad	0	0	0	
I_α[h]	amu.Å^2	3.12438483(20)	3.12438457(17)	3.122	
$\Delta I''$[h]	amu.Å^2	-0.51913(30)	-0.51933(26)	-3.606	
J''		12	12/163		
K_a''		6	6/41		
N_a[i]		304	304/3188		
RMS[j]	kHz	1.97	1.95/117.84		
WRMS[j]	Unitless	0.98	0.97/1.18		

[a] A, B and C in the ground state have been calculated at the “hybrid” level extrapolated at the CBS limit (see section computational methods for details). The centrifugal distortion constants Δ_J, Δ_{JK}, Δ_K, δ_J and δ_K have been calculated at the MP2/CBS level. The NQC constants χ_{aa}, χ_{bb} and χ_{cc} have been calculated at the B98/cc-pVQZ level. The internal rotation constants F and ρ have been estimated from A, B, C at the “hybrid” level and direction cosines λ_g and I_α estimated from the MP2/cc-pVQZ equilibrium structure. The $-CH_3$ internal rotation barrier V_6 have been calculated (ZPE corrected) at the MP2/CBS level. In all cases, the choice of the method is discussed in Ref. [17].

[b] P_a, P_b, P_c are the components of the overall rotation angular momentum, p_α is the angular momentum of the internal rotor rotating around the internal rotor axis by an angle α and $f(I,J,F)$ is the Casimir function. $\{u,v\}$ is the anti-commutator equal to: $uv+vu$. The product of the parameter and operator from a given row yields the term actually used in the vibration-rotation-torsion Hamiltonian, except for F, ρ, and A, which occur in the Hamiltonian in the form $F(p_\alpha-\rho P_a)^2+AP_a^2$. Like the internal axis of CH_3 is colinear with the a-axis, the RAM and PAM constants are equivalent.

[c] Recalculated from $A-\frac{B+C}{2}$, $\frac{B+C}{2}$ and $\frac{B-C}{2}$, note that theses constants defined in RAM are the same in PAM because the internal rotation axis i is coaxial with the a axis.

[d] Recalculated from $\chi_{aa}+\chi_{bb}+\chi_{cc}=0$ $(z=a, x=b, y=c)$, the standard deviation of χ_{bb} is calculated from the standard deviation of χ_{aa} and χ_{cc}.

[e] Recalculated from the fit of $-2\rho F$.

[f] Fixed to the calculated value.

[g] The $\angle(i,a)$ defined as the Euler angle δ which is the angle between the internal rotation axis i and the principal axis $z=a$.

[h] I_α is the inertia moment related to the $-CH_3$ internal top derived from $F=\hbar^2/2rI_\alpha$ in RAM36hf (see Eq. 2). $\Delta I''=I_c-I_b-I_a$ is the inertia defect related to the rotation of the molecular frame.

[i] Number of fitted a-type transitions.

[j] RMS and WRMS are the standard and the unitless standard deviations of the fit defined as: and with N the numbers of fitted lines and Δ_i the experimental error.

2.1.2. 2-Nitrotoluene

With the support of the quantum chemistry calculations presented in detail in supporting information (table S2), the jet-cooled MW spectrum (see section experimental methods) have been analysed up to $J'' = 9$ and $K_a'' = 5$ taking into account both the internal rotation of the methyl group and the NQC effects. The A species were preliminary assigned identically to the 4-NT analysis, using the SPFIT/SPCAT Pickett's programs[19] (semi-rigid rotor model in the I^r representation of A-reduced Watson's Hamiltonian). Then, the E species arising from internal rotation coupling of $-CH_3$ were assigned using the BELGI-C$_s$-hyperfine code, which is a slightly modified version of the BELGI-C$_1$-hyperfine code allowing to treat internal rotation effects with hyperfine structure for molecules with a planar frame.[26,27] Note that no c-type transitions were observed, which would have been consistent with a permanent dipole lying in the (a,b) plane in a C$_1$ structure (see Figure 4). In addition to the internal rotation splittings due to the $-CH_3$ group, additional splittings, likely due to the large amplitude motion (LAM) of the $-NO_2$ group have been observed in the 2-NT spectrum: 48 hyperfine components corresponding to 16 rotational transitions have been identified (see Table S3 of supplementary information II). Due to their limited number, these lines resulting from the $-NO_2$ torsion splitting were not included in the fit. Moreover, these splittings were very small (of about a few kHz to a few dozen of kHz, see Figure 5) and they were not always resolved.

The observed splittings for internal rotation coupling, NQC and Doppler doublets are small and very close, typically tens of kHz (see Figure 5), which leads to many overlapped signals. As a consequence, it was not possible to reach the experimental accuracy of 2 kHz for isolated lines, but a reasonable fit have been obtained considering 282 blended lines assigned to 390 transitions up to $J' = 10$ and $K_a'' = 5$, including 197 A species and 193 E species with a RMS deviation of 3.4 kHz. The

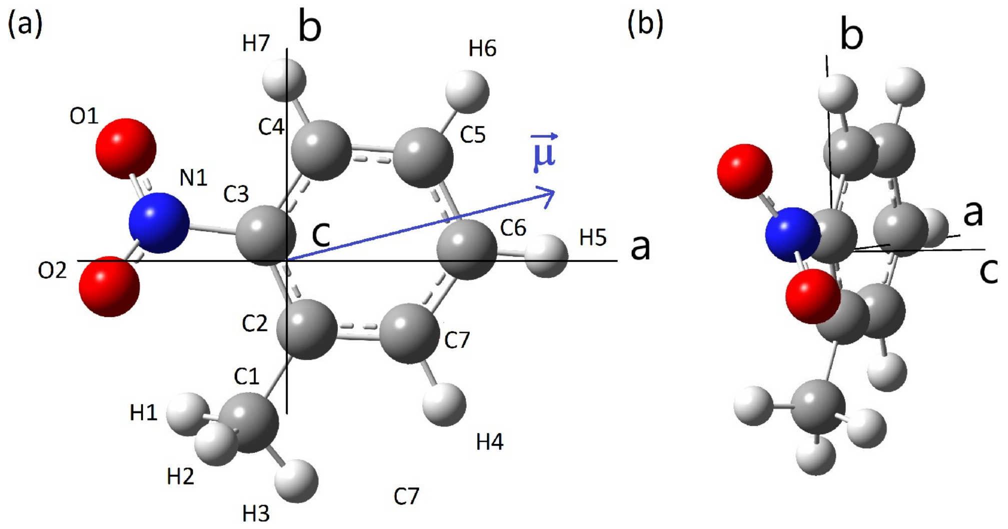

Figure 4. 2-NT geometry in the principal axis orientation optimized at the MP2/cc-pVQZ level of theory, (a) is a representation in the (ab) plane and (b) is tilted to show the out-of-plane $-NO_2$.

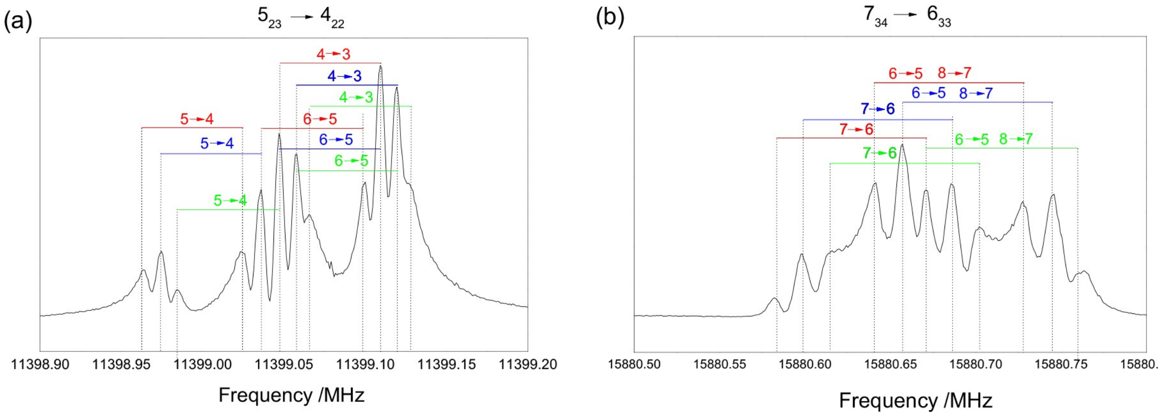

Figure 5. Experimental MW rotational lines of 2-NT for two ^aR-type transitions: (a) $5_{23} \rightarrow 4_{22}$ (200 coadded scans) and (b) $7_{34} \rightarrow 6_{33}$ (500 co-added scans). Doppler doublets have been assigned in the F'→F'' format for hyperfine transitions. The internal rotation splittings corresponding to the –CH3 internal rotation are identified in red for the A species and in blue for the E species. Additional splitting identified in green can be associated to the $-NO_2$ internal rotation.

complete set of molecular costants resulting from the analysis of 2-NT spectrum with the BELGI-C_s-hyperfine are presented in the supplementary Table S3 of supplementary information I. They are compared with quantum chemistry calculations in Table 2 after transformation from the Rho Axis Method (RAM) to the Principal Axis Method (PAM). Thirteen parameters were floated, the three rotational constants (*A, B, C*), four centrifugal distortion constants ($\Delta_J, \Delta_{JK}, \Delta_K, \delta_K$), the potential barrier height V_3, two higher order parameters c_1 and k_2 (see Table S3), the D_{ab} parameter and two NQC terms, χ_{aa} and χ_{cc}. The χ_{ab} NQC term was kept fixed to a value estimated from *ab initio* calculations and the other non-diagonal NQC terms were set to zero. Other parameters, such as the quartic centrifugal distortion term δ_J or higher order torsion-rotational parameters, were not well determined and they did not improve the fit, so we set their values to zero. While the RMS deviation is close to the experimental accuracy for the fit using the BELGI-C_s-hyperfine code, we noticed that the rotational constants and the NQC constants differ from their values obtained from quantum chemical calculations. On the contrary, the floated torsional parameters V_3, the derived inertia moment I_α of the $-CH_3$ group and the δ Euler angle are rather good agreement with those calculations, showing that the assigned splittings correspond to the $-CH_3$ internal rotation. Another fit was performed using the XIAM program[28,29] with the same line assignments. As shown in Table 2, the XIAM fit gives a RMS deviation of 3.5 kHz similar to the one obtained with the BELGI-C_s-hyperfine code. But with XIAM, the rotational and NQC parameters are in rather good agreement with the calculated values, while the values of the *F* internal rotation constant and ρ derived by XIAM are very different (see discussion section 2.3 which explains why the two fits complement each other).

Concerning the 2-NT room temperature mm-wave spectrum, the semi-rigid asymmetric rotor description of SPFIT/SPCAT Pickett's programs[19] was sufficient to carry out an analysis without considering any of the LAMs, internal rotation of $-CH_3$ or $-NO_2$ torsion. Indeed with such high barriers hindering these LAM motions, the line splittings are not resolved at the mm-wave spectrometer resolution. A total of 10746 transitions of A species corresponding to 7504 blended lines have been assigned up to $J''=187$ and $K_\alpha''=84$ using combination differences and the ASCP/SVIEW graphical interface of the AABS Package.[24,25] The global fit including only the MW and mm-wave A species allows to reproduce the spectra in the vibrational ground state with a very good unitless RMS of 1.03. The Figure 6 shows the good agreement between observed and simulated spectra in different parts of the mm-wave spectra. The molecular constants resulting from the mm-wave analysis of 2-NT using the SPFIT/SPCAT code are presented in Table 2. We can see that the mm-wave analysis allowed to improve the description of the semi-rigid rotor model including the determination of the two quartic constants kept fixed in the MW fit and all the sextic constants accurately determined.

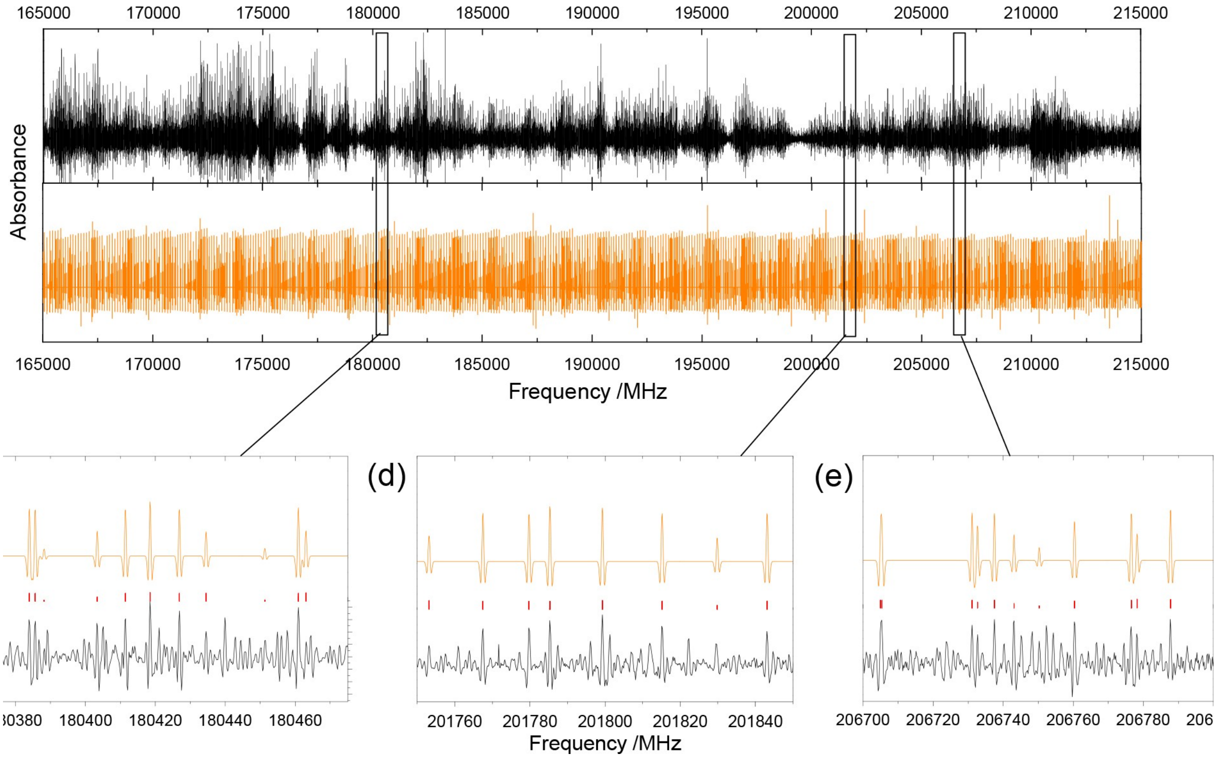

Figure 6. Part of the 70–330 GHz experimental mm-wave spectrum of 2-NT compared to the simulated spectrum obtained from the fit (see section 4.2): (a) is the 165 GHz–215 GHz experimental spectrum (black); (b) is the global simulated spectrum for the v = 0 ground state (orange). Some characteristics patterns of 2-NT are presented in (c), (d) and (e) with the individual frequencies calculated from the fit (red).

Table 2. Ground state torsion-rotation constants of the 2-NT obtained from the MW fit of A and E species (with BELGI-Cs-hyperfine and XIAM) and semi-rigid rotor constants obtained from the mm-wave/MW global fit of the A species (with SPFIT/SPCAT) are compared with quantum chemistry calculations. The numbers in parentheses represent one standard deviation in units of the least significant digit.

	Unit	BELGI-C_s-hyperfine MW (A and E species)	XIAM MW (A and E species)	SPFIT/SPCAT MW/mm-wave (A species)	Calc.[a]	Operator[b]
A	MHz	2205.4(137)[c]	2265.16372(68)[d]	2265.168753(101)	2268.664	P_a^2
B	MHz	1220.4(145)[c]	1247.2475(57)[d]	1247.2185033(268)	1240.220	P_b^2
C	MHz	829.32(45)[c]	834.2319(56)[d]	834.2641880(166)	841.059	P_c^2
Δ_J	kHz		0.06105(41)	0.06012280(211)	0.05899	$-P^4$
Δ_{JK}	kHz		−0.0461(41)	−0.0347652(184)	−0.0239	$-P^2P_a^2$
Δ_K	kHz		0.17906[f]	0.185629(143)	0.17906	$-P_a^4$
δ_J	kHz		0.01148[f]	0.01147527(99)	0.01148	$-2P^2\left(P_b^2-P_c^2\right)$
δ_K	kHz		0.2009(41)	0.1926039(218)	0.18765	$-\left\{P_a^2,\left(P_b^2-P_c^2\right)\right\}$
Φ_J	mHz			−0.010579(78)		P^6
Φ_{JK}	mHz			0.07526(100)		$P^4P_a^2$
Φ_{KJ}	mHz			−0.5100(38)		$P^2P_a^4$
Φ_K	mHz			1.0309(299)		P_a^6
ϕ_J	mHz			−0.010187(38)		$2P^4\left(P_b^2-P_c^2\right)$
ϕ_{JK}	mHz			−0.07722(57)		$P^2\left[P_a^2\left(P_b^2-P_c^2\right)+\left(P_b^2-P_c^2\right)P_a^2\right]$
ϕ_K	kHz			1.1609(42)		$\left[P_a^4\left(P_b^2-P_c^2\right)+\left(P_b^2-P_c^2\right)P_a^4\right]$
χ_{aa}	MHz	−1.077(21)[e]	−1.1518(32)[e]	−1.15068(256)	−1.3381	$2P_a^2(f(I,J,F)/J(J+1))$
χ_{bb}	MHz	0.340(25)[e]	0.4151(49)[e]	0.41417(58)	0.1788	$2P_a^2(f(I,J,F)/J(J+1))$
χ_{cc}	MHz	0.7367(38)[e]	0.7367(16)[e]	0.73651(316)	1.1593	$2P_c^2(f(I,J,F)/J(J+1))$
F	cm^{-1}	5.464[f]	0.711[g]		5.464	p_α^2
ρ	unitless	0.01000[f]	0.08386[g]		0.01085	$p_\alpha^2P^2$
V_3	cm^{-1}	686.3(34)	672(48)		645	$(1/2)(1-cos(3\alpha))$
$Dpi2-$	MHz		0.00078(7)[h]			$(p_\alpha-\rho P_r)^2\left(P_b^2-P_c^2\right)+\left(P_b^2-P_c^2\right)(p_\alpha-\rho P_r)^2$
δ[i]	rad	0.9251(113)	0.9678(277)		1.0655	
I_α[j]	amu.Å^2	3.115034(47)	25.8(18)		3.122	
$\Delta I''$[j]	amu.Å^2	−33.9(60)	−22.5031(22)	−22.5354788(66)	−29.372	
J''		9	9	9/187		
K_a''		5	5	5/84		
N_a[k]		300	300	300/10746		
N_b[k]		90	90	90/0		
RMS[l]	kHz	3.4	3.5	3.7/82.8		
WRMS[l]	unitless	1.7	1.7	1.9/1.03		

[a] A, B and C in the ground state have been calculated at the "hybrid" level extrapolated at the CBS limit. The centrifugal distortion constants Δ_J, Δ_{JK}, Δ_K, δ_J and δ_K have been calculated at the MP2/CBS level. The NQC constants χ_{aa}, χ_{bb} and χ_{cc} have been calculated at the B98/cc-pVQZ level. The internal rotation constants F and ρ have been estimated from A, B, C at the "hybrid" level and direction cosines λ_g and I_α estimated from the MP2/cc-pVQZ equilibrium structure. The –CH_3 internal rotation barrier V_3 is obtained from the 2D-PES along the two torsional angles (CH_3 and NO_2) calculated at the MP2/cc-pVTZ in the adiabatic path (see section 2.3 for more details).

[b] P_a, P_b, P_c are the components of the overall rotation angular momentum, p_α is the angular momentum of the internal rotor rotating around the internal rotor axis by an angle α, P_r is the angular momentum vector along the ρ axis (only used in XIAM) and $f(I,J,F)$ is the Casimir function. $\{u,v\}$ is the anti-commutator equal to: $uv+vu$. The product of the parameter and operator from a given row yields the term actually used in the vibration-rotation-torsion Hamiltonian, except for F, ρ, and A, which occur in the Hamiltonian in the form $F(p_\alpha-\rho P_a)^2+AP_a^2$.

[c] Recalculated from RAM to PAM using the D_{ab} operator (off-diagonal element of the inertial tensor in RAM system) fitted with the BELGI-C_s-hyperfine code.[26]

[d] Recalculated from the fitted constants $B_J=\frac{B_x+B_y}{2}$, $B_K=B_z-\frac{B_x+B_y}{2}$ and $B_-=\frac{B_x-B_y}{2}$ in XIAM in the I^r representation (z=a, x=b, y=c).

[e] χ_{aa} and χ_{cc} have been fitted and χ_{bb} calculated from $\chi_{aa}+\chi_{bb}+\chi_{cc}=0$. The BELGI-$C_s$-hyperfine NQC constants have been converted in PAM with a calculated non diagonal χ_{ab} kept fixed in RAM. The XIAM constants are recalculated from χ_{zz} and $\chi_-=\frac{\chi_{xx}-\chi_{yy}}{2}$ with $\chi_{xx}+\chi_{yy}+\chi_{zz}=0$.

[f] Fixed values estimated from the calculated value.

[g] Derived from the fitted values of $F_0=19.6(14)$ GHz, of the rotational constants (A, B, C) and of the $\delta=\angle(i,a)$ Euler angle (see Eq.(2)).

[h] Internal rotation overall-rotation distortion constant defined in XIAM.

[i] The $\angle(i,a)$ defined as the Euler angle δ which is the angle between the internal rotation axis i and the principal axis $z=a$. In BELGI-C_s-hyperfine, δ is obtained from $\tan\angle(i,a)=\frac{\lambda_b}{\lambda_a}=\frac{I_b}{I_a}\tan\theta_{RAM}$ with $\tan(2\theta_{RAM})=\frac{2D_{ab}}{B_{RAM}-A_{RAM}}$ obtained from the fit of D_{ab}, B and A in RAM.

[j] The inertia moment I_α related to the –CH_3 internal top is calculated from $F=\hbar^2/2rI_\alpha$ in BELGI-C_s-hyperfine (see Eq. (2)), and from $F_0=h^2/8\pi^2crI_\alpha=0.654(47)\ cm^{-1}$ in XIAM. $\Delta I''=I_c-I_b-I_a$ is the inertia defect related to the rotation of the molecular frame.

[k] Number of fitted a-type and b-type transitions are presented as N_a and N_b.

[l] RMS and WRMS are the standard and the unitless standard deviations of the fit defined as: $\sqrt{\frac{1}{N}\sum_i\left(f_i^{obs.}-f_i^{calc.}\right)^2}$ and with N the numbers of fitted lines and Δ_i the experimental error.

2.2. Nuclear quadrupole coupling

The two largest diagonal NQC constants, *i.e.* χ_{aa} and χ_{cc}, were used in the fit of 2-NT and 4-NT and the third diagonal constant (χ_{bb}) and its uncertainty were retrieved according to the traceless NQC tensor. Concerning the off-diagonal $\chi_{i,j,\ (j\neq i)}$ terms, none were added in the fits because only the most intense $\Delta F = \Delta J$ transitions were measured, which are insensitive to the off-diagonal constant. The calculated NQC tensor of 2-NT $\chi_{i,j}$ has been diagonalized in the principal axes system of the ^{14}N nucleus ($i, j = x, y, z$) in order to link the NQC constants to the molecular geometry and to the electronic structure ($\chi_{i,j} = eQq_{ij}$ with e the electric charge of the proton, Q the quadrupole moment and q_{ij} the molecular electric field gradient). Concerning the NQC tensor of 4-NT and the fitted NQC of 2-NT, the matrices were already diagonal and only identification of the NQC in the principal axis of the molecule to the principal axis of the nucleus was needed. The electric field gradient orientation can be evaluated using the asymmetry parameter η.[30] If the bond to the quadrupolar nucleus is axially symmetric ($\eta = 0$), it follows that $\chi_{xx} = \chi_{yy} = -\chi_{zz}/2$ due to the traceless coupling tensor and any deviation from axial symmetry reflects itself in a non-zero asymmetry parameter η. Therefore, a non-zero value of η would indicate significant deviations of the electric field gradient from the usually admitted cylindrical symmetry around the z-axis (coincident with the C–N bond here).

As can be seen from Table 3, most of the experimental and calculated (B98/cc-pVQZ) values of the relevant NQC constants for the three NT isomers poorly agree. Although DFT calculations of NQC constants for nitrogen containing molecules are usually accurate,[31] none of the most studied species contains a nitro group, for which difficulties were pointed out in an early study[32] and in the case of 3-NT.[17] Adding to this the rather complex treatment of an internal rotor, NQC results for the present species should be considered carefully. However, based on relative considerations only (*i.e.* considering that errors made are roughly the same for the three isomers), a strong isomeric dependence of the η parameter is observed with the experimental values while the calculated values are roughly the same. Indeed, experimental η increases as the methyl group gets farther from the nitro group (0.28, 0.45 and 0.55 for 2-NT, 3-NT and 4-NT, respectively) and thus converging to the calculated values (around 0.9 for the three isomers). For any reason difficult to assess, the influence of the methyl group on the electric field gradient around the quadrupolar nucleus clearly depends on the relative position of the functional groups in the benzene ring and this effect is not taken into account by the calculations.

2.3. Interaction between –CH_3 and –NO_2 in 2-NT

2.3.1. Anisotropic behaviour with a back-and-forth movement

The interaction between –CH_3 and –NO_2 has to be considered in the 2-NT "ortho" isomer, which appears as a peculiar case because of the immediate proximity of the two functional groups. Indeed, the equilibrium structure with the two groups tilted out the benzene plane, the surprisingly low barrier to –NO_2 internal rotation and the discrepancies between the values determined for the rotational and torsional parameters from our XIAM or BELGI-C_s-hyperfine fits compared to quantum chemical calculations are pointing toward some interaction between the torsional modes of these two groups. For these reasons, an exploration of the two-dimensional potential energy surface (2D-PES) along the two torsional angles has been performed at the MP2/cc-pVTZ level by mean of a relaxed scan procedure along C_3–C_2–C_1–H_1 dihedral angle at a given (fixed) value of the C_2–C_3–N_1–O_2 dihedral angle with 5° steps. To reduce the calculation time, scans were set to cover a 120° rotation of –CH_3 and a 180 rotation of –NO_2 and were then symmetrically expand to plot the complete surface (360°×360°) as shown in Figure 7 bottom-left panel. As expected, a standard 3-fold potential is observed along the –CH_3 rotation (equivalent minima and maxima every 120°). We also retrieve the "twisted" equilibrium positioning: the reference H atom is neither in the plane of benzene nor perpendicular but at 45°, this highlights the steric hindrance between the two groups. The –NO_2 rotation is more surprising: two different sequences reproducible at 180° are observed. Indeed, as –NO_2 is also "twisted",

Table 3. Fitted NQC constants $\chi_{i;j}$ in the principal axes system ($i, j = a, b, c$) for the NT isomers (including 3-NT from Ref.[17]) resulting from their global fit including MW and mm-wave transitions. Diagonalized $\chi_{i;j}$ in the principal axes system of the 14N nucleus ($i, j = x; y; z$) and asymmetry parameter η have been calculated for each set of parameters with their differential uncertainties on the last digit. The NQC constants of 3-NT were determined in Ref. [17].

		2-NT		3-NT		4-NT	
	Unit	Exp.	B98/cc-pVQZ	Exp.	B98/cc-pVQZ	Exp.	B98/cc-pVQZ
χ_{aa}	MHz	−1.15068(256)	−1.3381	−1.0494(16)	−1.244	−1.1724(62)	−1.3557
χ_{bb}	MHz	0.41417(58)[a]	0.1788	0.1986(91)[a]	−0.082	0.262(19)[a]	0.0387
χ_{cc}	MHz	0.73651(316)	1.1593	0.8507(20)	1.326	0.910(13)	1.317
χ_{ab}	MHz		0.1074	(−)0.4106(31)	−0.388		
χ_{ac}	MHz		−0.0164				
χ_{bc}	MHz		−0.371				
χ_{xx}	MHz	0.41417(58)	0.0610	0.3244(102)	0.036	0.262(19)	0.0387
χ_{yy}	MHz	0.73651(316)	1.2847	0.8507(20)	1.326	0.910(13)	1.317
χ_{zz}	MHz	−1.15068(256)	−1.3458	−1.17507(50)	−1.362	−1.1724(62)	−1.3557
η [b]	unitless	0.2801(57)	0.909	0.4479(106)	0.947	0.5527(365)	0.943

[a] Calculated according to $\chi_{aa} + \chi_{bb} + \chi_{cc} = 0$, standard deviation of χ_{bb} is calculed from the standard deviation of χ_{aa} and χ_{cc}.
[b] Asymmetry parameter $\eta = \frac{\chi_{xx} - \chi_{yy}}{\chi_{zz}}$.

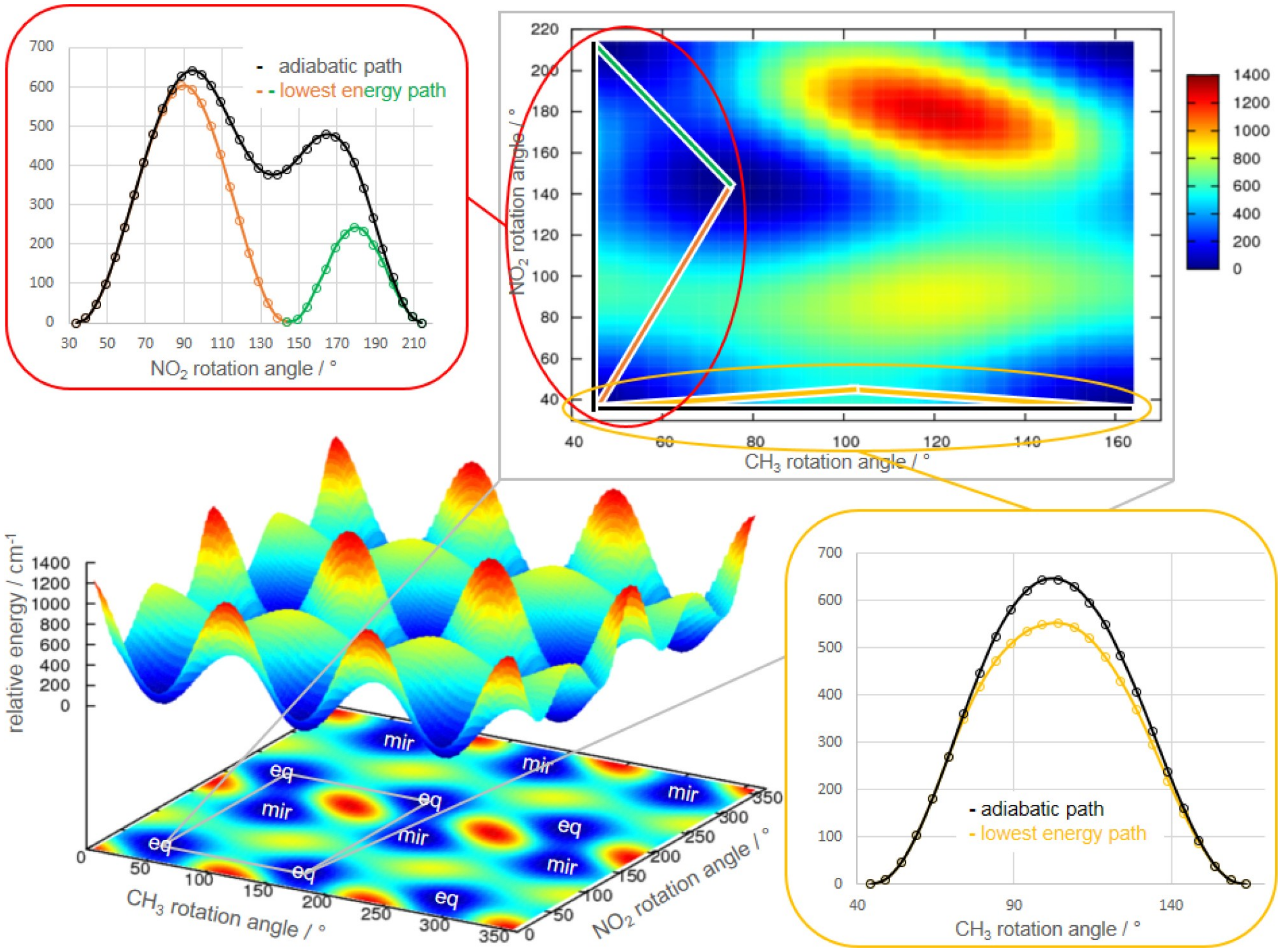

Figure 7. 2-D PES along the two torsional angles (–CH_3 and –NO_2) calculated at the MP2/cc-pVTZ level. Bottom-left panel: surface map plot for a complete rotation of both torsional groups; calculations were performed to cover a 120° rotation of CH3 and a 180° rotation of –NO_2 and then symmetrically expand to plot the complete surface. Top-right panel: top view in iso-surface format of an elementary area (120°–180°) of the surface between four equilibrium structures. Top-left panel: cuts of the PES for a 180° rotation of –NO_2 showing the adiabatic energy curve (in black) and the relaxed energy curve (in orange and green). Bottom-right panel: cuts of the PES for a 120° rotation of –CH_3 showing the adiabatic energy curve (in black) and the relaxed energy curve (in yellow).

there is an equilibrium structure at 35° (and 215°) from the plane of benzene (denoted "*eq*") and its mirror image at 180–35 = 145° (and 325°) (denoted "*mir*"), strictly iso-energetic. However, this mirror image is only possible if the –CH_3 group rotates accordingly (going from 45° to 120–45 = 75°), once again highlighting the interaction between the two functional groups.

The top-right panel of Figure 7 shows a top view (iso-surface format) of an elementary area (120°×180°) of the surface between four equilibrium structures. We clearly see that the paths of least energy to go from one equilibrium position (bottom-left corner) to the other (top-left or bottom-right corners) involve the movement of the two groups, but in an anisotropic manner:

- The top-left panel of Figure 7 shows cuts of the PES for a 180° rotation of –NO_2: the adiabatic energy curve, *i.e.* the vertical line corresponding to –CH_3 kept fixed at 45° (in black), and the relaxed energy curve, *i.e.* following the minimum energy points with –CH_3 free to move (in orange and green). The least energy (the latter) passes through the mirror image and therefore implies a non-negligible rotation of the –CH_3.
- The bottom-right panel of Figure 7 shows cuts of the PES for a 120° rotation of –CH_3: the adiabatic energy curve, *i.e.* the horizontal line corresponding to NO_2 kept fixed at 35 (in black), and the relaxed energy curve, *i.e.* following the minimum energy points with –NO_2 free to move (in yellow). In this case, the least energy (the latter) only implies a slight rotation of the –NO_2.

Figures 8a and 8b displays the relaxed energy curves, thus the least energy path, for a 180° rotation of –NO_2 and a 120° rotation of –CH_3; the dotted lines mark the variations of the angle of the –CH_3 and –NO_2 groups, respectively. The top panel shows the relevant molecular structures with in white the reference atoms considered for the measurement of dihedral angles compared to the plane of benzene. Denoting couples of angles as (CH_3, NO_2), the lowest energy path, starting from equilibrium (45°, 35°) towards the equivalent equilibrium (45°,

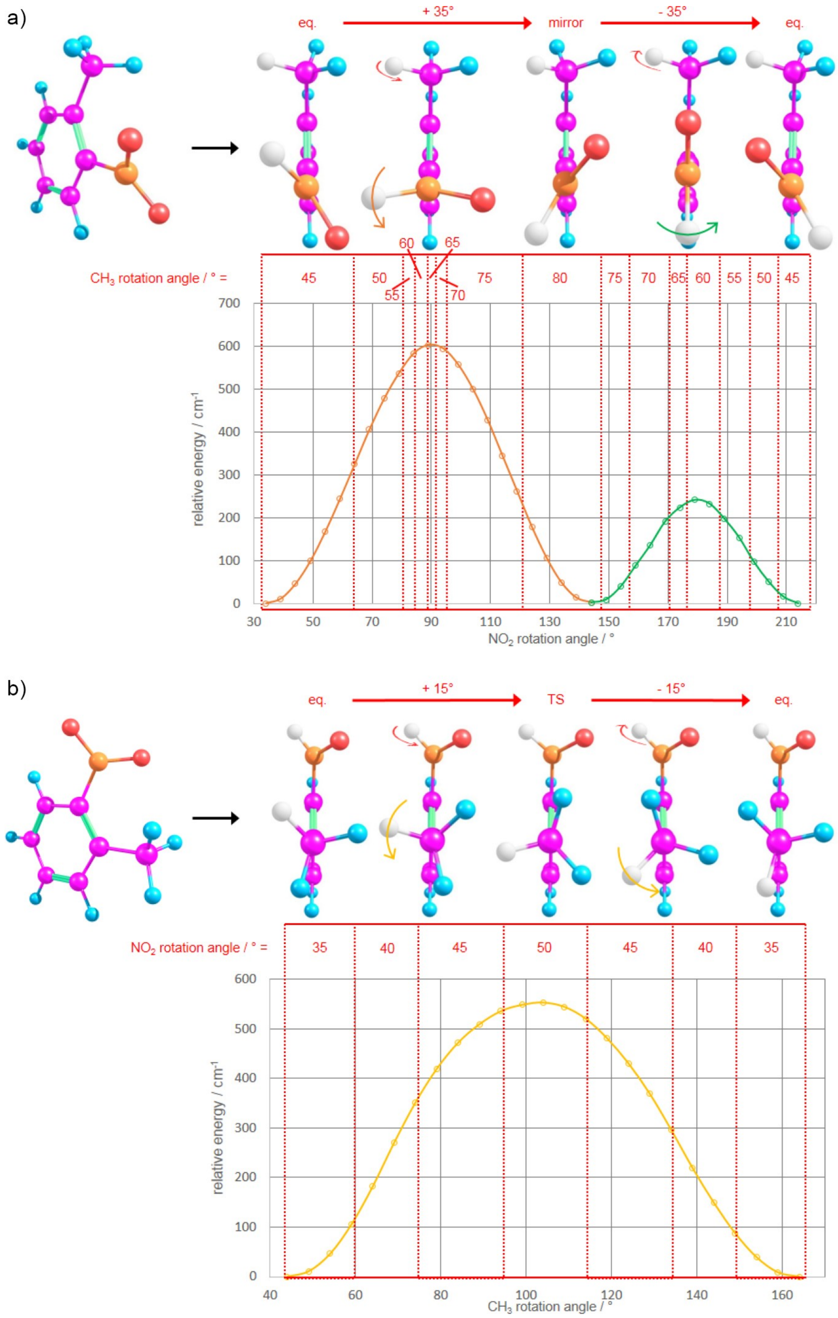

Figure 8. 2-NT lowest energy paths according to the –NO$_2$ (8a) and –CH3 (8b) LAMs and associated molecular structures. (a) Relaxed energy curve for a 180° rotation of –NO$_2$. The dotted lines separate the corresponding values of the angle of the –CH$_3$ group. The top panel shows the relevant molecular structures with in white the reference atoms considered for the measurement of dihedral angles compared to the plane of benzene. (b) Relaxed energy curve for a 120° rotation of –CH$_3$. The dotted lines separate the corresponding values of the angle of the –NO$_2$ group. The top panel shows the relevant molecular structures with in white the reference atoms considered for the measurement of dihedral angles compared to the plane of benzene.

215°), goes through three remarkable states which may be described for the –NO$_2$ rotation (Figure 8a) as: (i) a "perpendicular" transition state (60°, 90°) = 604 cm^{-1}, (ii) an iso-energetic mirror image of the equilibrium (75°, 145°) and (iii) an "in plane" transition state (60°, 180°) = 233 cm^{-1}. While –NO$_2$ twists towards the perpendicular position, it leaves room for the methyl to take its symmetrical position. Then, after a 90° rotation, the opposite oxygen atom pushes the methyl towards its mirror image such that it will have rotated by 35°. By continuing to twist to the equivalent position (+180°), –NO$_2$ pushes the methyl in an opposite rotation to bring it back to the initial position (45°) passing by the "in plane" transition state. The 180° rotation of –NO$_2$ is therefore accompanied by a back-and-forth movement of the methyl over an amplitude up to 35°.

Figure 8b displays the least energy path for a 120° rotation of $-CH_3$. In this case, the situation is more simple since, starting from equilibrium (45, 35) towards the equivalent position (165°, 35°), the path of least energy does not pass through a mirror image. The $-CH_3$ rotation over 120° is accompanied by a smaller back-and-forth movement of the nitro group, with an amplitude of 15°, inducing a rotation barrier of 553 cm^{-1}, slightly lower compared to the adiabatic path: 645 cm^{-1}. It is quite interesting to note that the experimental values for the barrier height hindering the $-CH_3$ internal rotation ($V_3 = 672(48)\ cm^{-1}$, and $V_3 = 686.3(34)\ cm^{-1}$ deduced from the fits of the XIAM code and the BELGI-C_s-hyperfine code, respectively) are in very good agreement (6% for BELGI-C_s-hyperfine and 4% for XIAM) with the *ab initio* barrier height calculated with the adiabatic path.

2.3.2. Discussion on the molecular parameters

The BELGI-C_s-hyperfine and XIAM fits have provided rotational constants with significant differences: 2.7%, 2.2%, 0.6% differences for *A, B* and *C*, respectively, if we compare the XIAM constants with respect to those of BELGI-C_s-hyperfine. Nevertheless, both fits and quantum chemical calculations provide a strong negative inertial defect $\Delta I''$[33] induced by the out of plane tilted $-NO_2$ group. With a deviation of 1.5% for *A*, 1.6% for *B*, and 0.8% for *C*, the rotational constants obtained from the XIAM fit agree well with the $A_0,\ B_0,\ C_0$ constants calculated at the "hybrid" level (see section computational methods). In comparison, the rotational constants obtained from the BELGI-C_s-hyperfine code do not match so well (−2.9%, −1.6% and −1.4% for *A, B* and *C*, respectively). These differences are due to the fact that the XIAM and BELGI-C_s-hyperfine are based on two different models (see section methods to analyse the LAMs). As a consequence, different sets of parameters are used in XIAM and BELGI. Then, the conversion of some RAM parameters to PAM parameters is not unique and introduces some errors when trying to compare the parameters with each other. In the XIAM code, we note in Table 2 the very unusual values of the internal rotation parameter *F* of 0.711 cm^{-1}, corresponding to an extremely high value for the moment of the inertia of the $-CH_3$ top $I_\alpha = 25.8(18)$ amu.Å^2 (instead of the "more classical" calculated value of 3.12 amu.Å^2 for a $-CH_3$), as well as the rather large value of the ρ parameter of 0.08386 which is around 8 times larger than the calculated value and that was used in the BELGI-C_s-hyperfine fit. Both *F* and ρ are non fitted parameters. They are derived in XIAM from Eq. (2) and from the Euler angle between the principal axis *a* and the internal axis of the top, ($\delta = \angle(i, a) = 0.9678(277)\ rad.$, see Table 2). Therefore, the I_α XIAM value correspond to a "dummy" heavier internal top reflecting the influence of the $-NO_2$ internal rotation. On the other hand, in the BELGI-Cs-hyperfine code, we do not fit directly any angle. Instead, we float the D_{ab} parameter which is related to the off-diagonal terms in the inertia tensor. The value for the $\delta = 0.9251(113)$ angle is obtained by diagonalizing this inertia tensor. Moreover, in the present study, with experimental data originating only from the ground torsional state $v_t = 0$, the internal rotation parameters are highly correlated and we have to fix the values of *F* and ρ to their calculated values. Finally, none of the codes used in this study take into account explicitly the coupling of a methyl internal rotation and the back-and-forth LAM motions of the $-NO_2$ group. With the 2-NT molecule, we are facing a rather complex case of coupled LAMs due to existence of two relatively high barrier of similar magnitude (672 cm^{-1} for the three-fold potential V_3 of the CH_3 and 604 cm^{-1} for the two-fold potential V_2 of the $-NO_2$).

2.4. Influence of the isomery on the methyl group internal rotation

Table 4 reports the $-CH_3$ internal rotation barrier constants V_3 and/or V_6 in mono-substituted toluene derivatives with various substituents in ortho (o-), meta (m-) and para (p-) positions determined experimentally in the literature by different spectroscopic techniques. For the ortho isomers, all the $-CH_3$ internal rotation barriers are rather high with V_3 constants of several hundreds of wavenumbers. The different V_3 values are consistent with a steric hindrance increasing more or less the barrier according to the close neighbouring functional group. Moreover, we can notice that only MW experiments have been performed for these ortho isomers allowing the sole determination of the V_3 constant and no higher order term such as V_6 is available. This can be explained by two reasons: (i) internal rotation splittings of rotational transitions in the excited torsional states are required to determine these higher order terms but the jet-cooled conditions prevent their observation and (ii) the internal rotation splittings are usually very small for high internal rotation barriers and are only resolved by Fabry-Pérot Fourier-transform microwave (FP-FTMW) experiments. For the meta and para isomers, the V_3 and/or V_6 barrier constants are very low and never exceed few tens of wavenumbers. Notably, few spectroscopic studies (mainly meta isomers analyses) determined both V_3 and V_6 in their description of the internal rotation potential. Only our 3-NT study combining jet cooled FP-FTMW and room temperature mm-wave data in Ref. [17] was able to determine both terms with a high degree of accuracy. Finally, most of the para isomers belong to the C_{2v} symmetry group, so the V_6 constants are solely fitted. The V_6 term in toluene reflects the difference in potential energy for a C-H bond of the methyl group lying in the ring plane or lying in a plane perpendicular to the ring plane.[34] Similar values for V_6 are found for p-chlorotoluene, p-fluorotoluene and p-toluidine. Interestlingly the value for the V_6 term in 4-NT is almost 2.5 times bigger than for those species, showing that the methyl group barrier is sensitive to the existence of a $-NO_2$ resonance group located at the other part of the molecule versus a local symmetry effect at the methyl site itself. A V_3 potential appears when the C_{2V} symmetry is broken by a non symmetric substituent. One example is the para-tolualdehyde study where information on the broken C_{2v} symmetry by the aldehyde functional group at the top of the ring being transmitted to the methyl-group site at the bottom of the ring can be obtained by quantifying the influence of the aldehyde group on the internal rotation barrier seen by the methyl group.[34]

Table 4. V_3 and V_6 constants of mono-substituted toluene derivatives (ortho, meta and para isomers).

Molecule	Substituent	V_3[c]/cm^{-1}	V_6[c]/cm^{-1}	Type of spectroscopy	Ref.
o-chlorotoluene	–Cl	466.2(15)	–	MW	[56]
o-fluorotoluene	–F	227.28(2)	–	MW	[57]
o-toluidine	$-NH_2$	531(7)	–	MW	[58]
o-nitrotoluene	**$-NO_2$**	**686.3(34)/672(48)[a]**	–	**MW/mm-wave**	**This work**
o-xylene	$-CH_3$	521(17)	–	MW	[59]
o-Tolunitrile	–CN	187.699(3)	–	MW	[29]
o-cresol (trans)	–OH	369.95(11)	–	MW	[60]
o-cresol (cis)	–OH	661.4(38)	–	MW	[60]
o-cresol-OD (trans)	–OD	371.046(40)	–	MW	[60]
o-cresol-OD (cis)	–OD	669.10(50)	–	MW	[60]
o-methylanisole	$-OCH_3$	444.48(42)	–	MW	[61]
m-chlorotoluene	–Cl	2.452/3.2398(50)[d]	17.197(36)/-10.991[d]	MW	[62]
m-fluorotoluene	–F	20.20(45)	−7.70(41)	electronic	[63]
m-toluidine	$-NH_2$	1.97(5)	–	MW	[58]
m-nitrotoluene	**$-NO_2$**	**6.7659(24)**	**0.02333(22)**	**MW/mm-wave**	**Previous work[17]**
m-xylene	$-CH_3$	4.49(14)	–	MW	[64]
m-tolunitrile	–CN	14.1960(3)	−11[e]	MW	[65]
m-cresol (trans)	–OH	3.2(2)	−13.88(15)	MW	[66]
m-cresol (cis)	–OH	22.44(7)	−11.2(8)	MW	[66]
m-cresol-OD (trans)	–OD	3.188(180)	–	electronic	[67]
m-cresol-OD (cis)	–OD	21.341(52)	–	electronic	[67]
m-tolualdehyde (cis)	–CHO	35.925(3)	–	MW	[68]
m-tolualdehyde (trans)	–CHO	4.64(3)	–	MW	[68]
m-methylanisole (cis)	$-OCH_3$	55.7693(90)	–	MW	[69]
m-methylanisole (trans)	$-OCH_3$	36.6342(84)	–	MW	[69]
toluene	–	none[b]	4.83783988(48)	MW/mm-wave	[21]
p-chlorotoluene	–Cl	none[b]	4.873(13)	MW	[70]
p-fluorotoluene	–F	none[b]	4.8298(63)	MW	[71]
p-toluidine	$-NH_2$	none[b]	±5.6[e]	electronic	[72]
p-nitrotoluene	**$-NO_2$**	**none[b]**	**12.22(18)**	**MW/mm-wave**	**This work**
p-xylene	$-CH_3$	none[b]	10[e]	electronic	[73]
p-tolunitrile	–CN	none[b]	−10[e]	electronic	[74]
p-cresol	–OH	18.39(3)	−7.3(6)	MW	[75]
p-tolualdehyde	–CHO	28.111(1)	−4.768(7)	MW	[34]
p-methylanisole	$-OCH_3$	49.6370(1)	–	MW	[76]

[a] the two values correspond to the barrier fitted with BELGI-C_s-hyperfine/XIAM code.
[b] because of the C_{2v} symmetry of the molecule.
[c] "–" if no value is explicitly given for V_3 or V_6.
[d] two fits have been performed in Ref.[62]: one with V_3 fixed to MP2/6-311++G(2d,2p) calculation, the other with V_6 fixed to the same level.
[e] values found in the literature without uncertainties.

3. Conclusions

The rotational spectra of two TNT explosive taggants, the 2-NT and 4-NT, have been measured and analyzed by jet-FTMW and mm-wave room temperature rotational spectroscopies. Combined with quantum chemistry calculations, the MW study allowed to describe the lowest rotational energy levels of the molecules taking into account both the internal rotation coupling of the $-CH_3$ group and the NQC involved by the ^{14}N nucleus in the $-NO_2$ group. In the mm-wave spectral domain, an important congestion of the rotational lines is mainly due to the presence of hot bands involving the low-lying vibrational modes populated at room temperature: most of the lines are blended, hyperfine structures and 2-NT internal rotation splittings are not resolved. Concerning the analysis of the MW and mm-wave spectra of 4-NT, larger internal rotation splittings have been observed with a low internal rotation barrier ($V_6 = 12.22(18)$ cm^{-1}), the spin statistics has been calculated to reproduce the line intensities and the NQC have also been analysed from the MW transitions. The analysis of 2-NT MW line splittings was particularly complicated and challenging due to the coupling of the neighbored $-CH_3$ and $-NO_2$ torsional motions characterized by two barriers with closed amplitudes ($\simeq$680 cm^{-1}). Quantum chemistry calculations performed in this study have revealed a unexpected anisotropic behaviour with a back-and-forth movement of the methyl/nitro double torsion. The two different adiabatic internal rotation models BELGI-Cs-hyperfine and XIAM reproduce the splitting due to NQC and $-CH_3$ internal rotation close to the experimental accuracy but not those due to $-NO_2$ internal rotation observed only in 16 MW lines. Nevertheless, with such rather high internal rotation barriers, it was not necessary to take into account these internal rotation effects at the resolution of the frequency multiplication chain in order to reproduce the most intense mm-wave lines of the 2-NT vibrational ground state spectrum. From a fundamental point of view, the NT rotational analyses produced in this study and in Ref. [17] associated with other high-resolution spectroscopic studies explain the isomeric influence on the internal rotation barriers in the mono-substituted toluene derivatives.

For future work it will be important to extend the multi-dimensional coupling of LAMs in theoretical effective Hamiltonians models by taking into consideration a C_1 frame coupled with two non equivalent LAMs in a gearing back-and-forth motion. In the 2-NT mm-wave spectrum, it could allow to analyse torsional splittings potentially resolved for higher torsional levels (with $v_t \geq 1$) in order to decrease the correlations between various parameters in the Hamiltonian and to permit the determination of higher order terms (V_6, V_9…) of the potential hindering the internal rotation. From a more applied point of view, mm-wave rotational lines list, produced for the three NT isomers and provided in electronic supplementary information II (see Tables S1, S2, S4 and S5), are crucial for a future monitoring of these explosive taggants in realistic conditions. As an example, the transition frequencies of the strongest lines may be used for an unambiguous recognition of the NT even in a vapor mixture with the different isomers (see Figure S3 in supplementary information I). However, taking into account the experimental difficulties to measure at room temperature the rotational signatures of these weakly volatile taggants, the ability to perform field measurements of NT vapor traces requires important improvements of the mm-wave spectrometers in terms of sensitivity. Nevertheless, recent technological breakdowns based on intra-cavity techniques[35,36] push the detection limits while preserving the incomparable selectivity of the high-resolution mm-wave rotational spectroscopy.

Experimental and theoretical methods

Jet-cooled FP-FTMW spectroscopy

The 2-NT (liquid at 293K) and 4-NT (solid at 293K) have been purchased from Aldrich Chemistry with high level of purity (of $\geq 99\%$). The NT spectra have been measured in the MW region (2-20 GHz) using the FP-FTMW technique coupled to a pulsed supersonic jet.[37,38] A heated nozzle[39] allowed to mix the NT vapour with the carrier gas (neon) at a backing pressure of about 0.2 MPa. Temperatures ranging from 373 K to 393 K were found to optimize the S/N ratio depending on the amplitude of recorded lines. The mixture was introduced into the FP cavity through a series 9 General Valve pin hole nozzle (0.8 mm) at a repetition rate of 1.5 Hz. Jet-cooled molecules (T_{rot} of a few K) were polarized within the supersonic expansion by a 2 μs pulse. The free-induction decay (FID) signal is recorded using heterodyne detection at 30 MHz, and is digitized at a repetition rate of 120 MHz on a 14 bit resolution electronic card. FID signals were accumulated between 50 and 1000 times, depending on the line intensity. After Fourier transformation of the average FID, rotational lines of the amplitude spectrum were observed as Doppler doublets due to the coaxial arrangement of the jet and the FP cavity. Each resonance frequency was measured as the average frequency of the two Doppler components. The spectral resolution is depending on the number of recorded points. The frequency grid was set to 1.8 kHz, which was found sufficient since the Doppler linewidths should be of several kHz. According to this value, the experimental accuracy of the MW measured lines was estimated to 2 kHz.

Room temperature mm-wave spectroscopy

The room temperature absorption spectra of NT isomers have been measured in the mm-wave region (70-330 GHz and 70-230 GHz for the 2-NT and 4-NT, respectively) using a frequency multiplication chain.[40] A continuous flow of 8 μbar of the sample, maintained by a roughing pumping, was passed through a 125 cm-long and 56 mm-diameter double path stainless steel absorption cell equipped with Teflon windows and probed by the radiation generated by a frequency multiplier chain (Virginia Diodes, Inc). Two off-axis parabolic mirrors are used to collimate the radiation into the cell and then to refocus it into a liquid helium cooled InSb bolometer. Compared to the previous single pass cell configuration detailed in Ref. [17] the double pass configuration developped by adding a rooftop mirror and a grid in Ref. [41] allowed to improve the S/N ratio of the molecular transitions. The spectra have been recorded in 2F frequency modulation by using a frequency modulation of 10 kHz, a modulation depth of 33 kHz, a time constant of 50 ms for the 140–330 GHz region recorded with the InSb bolometer and 200 ms for the 70–110 GHz range recorded with a Schottky diode. Frequency steps have been adjusted from 100 kHz to 150 kHz following the frequency dependence of the Doppler linewidth in the 70–330 GHz scanned range. A post treatment of the mm-wave spectra have been successfully applied with a low-pass FFT filter subtraction to simulate and remove the strong baseline variations arising from stationary waves between the source, the cell and the detector.[17] The obtained spectra are very dense, weak and complicated by the presence of rotational transitions in many low-lying vibrational states populated at room temperature and by the congestion of the lines which are mostly blended. The mm-wave line accuracy has been estimated to 80 kHz and 100 kHz for the 2-NT and 4-NT, respectively, according to the average S/N ratio of the measured lines.[42]

Computational methods

Geometries and symmetries

All geometries were fully optimized at the MP2 and B98 levels with a tight convergence criterion using Gaussian 16 rev B.01 software[43] on the computing cluster of PhLAM laboratory. The frozen-core approximation was used throughout. Extrapolations to complete basis set (CBS) for energies (including Zero Point Energy (ZPE) corrections) and rotational constants were performed using Dunning and coworkers formula[44] and correlation consistent basis set cc-pVXZ (X = D, T, Q).[45] Vibrational frequencies and ground state ($v = 0$) rotational constants were calculated at the anharmonic level (VPT2 calculations as implemented in the Gaussian software)[46] with a tight SCF convergence criterion and the ultrafine integral grid option. Anharmonic corrections have been extrapolated from DFT (B98 functional) to the MP2 level following a method suggested by Barone *et al.*[47] and recently successful in the case of various systems,[48] including internal rotors[17,49] (denoted "hybrid" hereafter, see Refs for details).

The geometry of 2-NT and 4-NT optimized at the MP2/cc-VQZ level of theory is presented in Figs. 1 and 4, respectively. A strong permanent dipole moment is expected for the two molecules with $\mu \simeq 4.8$ D in the (a,b) plane for 2-NT ($\mu_a \simeq 4.7\ D$ and $\mu_b \simeq 0.8\ D$) and $\mu \simeq 5.8$ D along the a-axis for 4-NT. They are both prolate tops with a strong asymmetry for 2-NT ($\kappa = -0.44$) and a slight asymmetry for 4-NT ($\kappa = -0.91$). Concerning 2-NT, the equilibrium structure shows a G_3 permutation inversion (PI) symmetry with a C_1 frame and a C_{3v} top for the methyl group. [50] This can be explained by a steric repulsion between the $-CH_3$ and $-NO_2$ which twists the $-NO_2$ out of the plane of the benzene ring (see Figure 4 (b)). For 4-

NT, the equilibrium structure calculated at the MP2/cc-pVQZ level of theory shows a G_{12} PI symmetry with a C_{2v} molecular frame and a C_{3v} top for the methyl group. [20] In opposite to 2-NT and 3-NT, the G_{12} symmetry of 4-NT leads to equivalent atoms and thus to a nuclear spin statistics which affect the intensity of the lines according to the (A1/A2, B1/B2, E1, E2) species of the G_{12} PI group. The degeneracy has been determined considering four equivalent hydrogens with a nuclear spin of $I=1/2$ (permutations ($H4 \leftrightarrow H5$) and ($H6 \leftrightarrow H7$)), four equivalent carbons with $I=0$ (permutations ($C1 \leftrightarrow C2$) and ($C3 \leftrightarrow C4$)) and two equivalent oxygens with $I=0$ (permutations ($O1 \leftrightarrow O2$)) (see Figure 4 for the labels). For each equivalent atom, $(2I+1)(I+1)$ symmetric and $(2I+1)I$ antisymmetric nuclear spin eigenfunctions have been identified using the G_{12} PI group[20] and the total nuclear spin eigenfunction Ψ_{ns} has been determined from the total $(C1 \leftrightarrow C2)(C3 \leftrightarrow C4)(H4 \leftrightarrow H5)(H6 \leftrightarrow H7)(O1 \leftrightarrow O2)$ permutations. Finally, the statistical weight have been determined to (5, 3, 3, 5) from the Pauli principle application to $\Psi_{tot} = \Psi_{el}\Psi_{vib}\Psi_{rot}\Psi_{ns}$ which correspond to a symmetric total eigenfunction.

Internal rotation couplings

In order to have an initial prediction of the frequency splitting arising from the internal rotation coupling of $-CH_3$, it was necessary to estimate the main torsional parameters $V(\alpha)$, F and ρ. These parameters correspond to the barrier height, the internal rotation constant and a coupling constant between rotation and torsion, respectively.[51] Firstly, the potential function $V(\alpha)$ can be expressed as a Fourier series in terms of the torsional angle α and of the number of equivalent positions n of the methyl group torsion:[51]

$$V(\alpha) = \frac{1}{2}V_n(1 - cos(n\alpha)) + \frac{1}{2}V_{2n}(1 - cos(2n\alpha)) + ..., \qquad (1)$$

The first term in Eq. 1 includes the barrier height V_n, with $n=3$ for 2-NT and $n=6$ for 4-NT. The barrier height values were estimated at the MP2 level by optimizing the transition state of the methyl group rotation (QST2 method as implemented in Gaussian16), then extrapolated at the CBS limit and ZPE corrected from harmonic frequency calculations at equilibrium and transition state optimized geometries. A barrier of $V_3 = 501\ \mathrm{cm}^{-1}$ has been calculated for 2-NT and $V_6 = 11.3\ \mathrm{cm}^{-1}$ for the 4-NT. Then, the internal rotation constant F and the ρ_g components (with $g = a, b, c$) of the ρ vector have been calculated from the principal moments of inertia of the molecule I_g, the moment of inertia of the internal top I_α and the direction cosines λ_g of the internal rotation axis i in the principal axis system (i.e. $\lambda_g = cos(\theta(i,g))$) derived from the MP2/cc-pVQZ equilibrium structure with the expressions: [51]

$$\rho_g = \lambda_g \frac{I_\alpha}{I_g} \quad F = \frac{\hbar^2}{2rI_\alpha} \quad r = 1 - \sum_g \lambda_g^2 \frac{I_\alpha}{I_g} \qquad (2)$$

Additional calculations at the MP2/cc-pVTZ level have been performed to calculate the internal rotation barrier height of the $-NO_2$ group for the three isomers (transition state energy from QST2 method). As for 3-NT, [17] the $-NO_2$ group of 4-NT can be considered as rigid compared to the molecular frame with $V_2 = 1692\ \mathrm{cm}^{-1}$ (ZPE corrected). For 2-NT, an unexpected value of $V_2 = 443\ \mathrm{cm}^{-1}$ has been calculated, leading to a lower barrier than the 2-NT $-CH_3$ internal rotation barrier. Considering the short distance between $-NO_2$ and $-CH_3$ (close neighbors in the benzene ring), an interaction between the two groups might be expected. Therefore, the 2D-PES of total electronic energy has been calculated at the MP2/cc-pVTZ level for a complete rotation of $-CH_3$ and $-NO_2$ with steps of 5. As suggested by the equilibrium structure showing tilts of the two functional groups out of the plane of benzene (see Figure 4), a clear interaction between the two groups is evidenced by the PES calculation (see section 2.3 for complete discussion).

Nuclear quadrupole coupling

Concerning the NQC of the electric field gradient tensor induced by the coupling with the ^{14}N nuclear spin ($I=1$) of 2-NT and 4-NT, large differences have been observed between MP2 and B98 results. This difference was also observed in the study of 3-NT with a nitrogen in NO_2 which behaves as if it is quadruply bonded to a dummy atom (equivalent to the two oxygen atoms) of lower electro-negativity.[17,52,53] Based on additional calculations at the B2PLYP, B3PW91 and MP2(full) levels of theory with specific basis-set, it was established for 3-NT in Ref. [17] that MP2 and MP2(full) failed in predicting correctly NQC constants, independently from the size of basis set. Considering that the Density Functional Theory (DFT) methods B2PLYP, B98 and B3PW91[31] can provide reliable results with relative uncertainties of few %, the hyperfine constants calculated at the B98/cc-pVQZ level of theory have been used for the analysis of the hyperfine splittings in MW spectra of 2-NT and 4-NT, as in the case of 3-NT.

Methods to analyse the LAMs

In the frame of the various methods which describe the LAMs effects, effective rotation torsional Hamiltonian are set up in either the PAM or in the RAM. The RAM allows us to eliminate at the zero order certain coupling terms in the kinetic energy between the internal angular momentum p_α and the global rotational momentum P, and to simplify the diagonalization of the Hamiltonian.[26,51] This approach is used in the BELGI series of codes,[26,27,54,55] as well as in the RAM36hf code[20,21] of which a version will be used in the 2-NT and 4-NT spectra analyses, respectively. The molecular parameters obtained by those two approaches can be transformed into the PAM by an angle called θ_{RAM}.[54] A first estimation of θ_{RAM} can thus be obtained from the *ab initio* equilibrium structure. In other codes such as XIAM[28,29] (used also in the 2-NT study), the internal rotation operator is also set up in the RAM but the eigenvalues and molecular parameters are transformed back from the PAM via a rotation about the Euler angles δ and γ which have been firstly estimated from the optimized equilibrium structure. The difference between the XIAM code and the BELGI/RAM36 codes lies in the fact that XIAM treats the A and E species of each torsional v_t state set by itself, with different sets of parameters for each v_t state ("*local methods*"), whereas BELGI/RAM36 treat all the torsional manifold v_t states from a given vibrational state together, and diagonalize the matrix of the torsional-rotational Hamiltonian containing thus all the interactions between the torsional states ("*global methods*").[26]

Acknowledgements

We thank Vadim Ilyushin from the Institute of Radio Astronomy of NASU (Ukraine) for the modification of its RAM36hf code to extend the energy level calculations from $J = 100$ to $J = 180$ for the mm-wave spectral analysis of 4-NT and H. V. Lam Nguyen from the Université Paris-Est Créteil & Université de Paris for her recommendations and tests in the XIAM fit of 2-NT. Marc Fourmentin from the Université du Littoral Côte d'Opale (LPCA) for the design of the cover feature. We thank the PhD financial supports of A. Roucou, i.e. the region Hauts-de-France and the French Délégation

Générale pour l'Armement (DGA), and the PhD financial supports of S. Bteich, i.e. the region Hauts-de-France and the Laboratory of Excellence CaPPA (Chemical and Physical Properties of the Atmosphere) funded by the French National Research Agency (ANR) through the PIA (Programme d'Investissements d'Avenir) under Contract No. ANR-11-LABX-005-01. A. Roucou was funded by the "Groupe de Recherche GdR SPECMO" to visit I. Kleiner in LISA, Créteil. The mm-wave spectrometer has been supported by the French "Délégation Générale pour l'Armement" (Projet de Recherche Exploratoire et Innovation No. 06.34.037).

Conflict of Interest

The authors declare no conflict of interest.

Keywords: Explosive taggant · Large amplitude torsions · Molecular dynamics · Nitrotoluene isomers · Rotational spectroscopy

[1] H. Östmark, S. Wallin, H. G. Ang, *Propellants Explos. Pyrotech.* **2012**, *37*, 12–23.
[2] D. S. Moore, *Rev. Sci. Instrum.* **2004**, *75*, 2499–2512.
[3] A. R. Krause, C. Van Neste, L. Senesac, T. Thundat, E. Finot, *J. Appl. Phys.* **2008**, *103*, 094906.
[4] M. Snels, T. Venezia, L. Belfiore, *Chem. Phys. Lett.* **2010**, *489*, 134–140.
[5] R. Prasad, R. Prasad, G. Bhar, S. Thakur, *Spectrochim. Acta Part A* **2002**, *58*, 3093–3102.
[6] A. G. Mercado, J. A. Janni, B. Gilbert, *SPIE Proc.* **1995**, *2511*, 142–152.
[7] D. Wu, J. P. Singh, F. Y. Yueh, D. L. Monts, *Appl. Optics* **1996**, *35*, 3998–4003.
[8] C. Mullen, A. Irwin, B. V. Pond, D. L. Huestis, M. J. Coggiola, H. Oser, *Anal. Chem.* **2006**, *78*, 3807–3814.
[9] H. Diez y Riega, R. Gunawidjaja, H. Eilers, *J. Photochem. Photobiol. A* **2013**, *268*, 50–57.
[10] Convention on the marking of plastic explosives for the purpose of detection, signed at montreal, on 1 march 1991 (montral convention 1991).
[11] Y. Chen, H. Liu, Y. Deng, D. B. Veksler, M. S. Shur, X.-C. Zhang, D. Schauki, M. J. Fitch, R. Osiander, C. Dodson, et al. *P. Soc. Photo.-Opt. Ins.* **2004**, *5411*, 1–9.
[12] S. Letzel, T. Göen, M. Bader, J. Angerer, T. Kraus, *Occup. Environ. Med.* **2003**, *60*, 483–488.
[13] A. Cuisset, S. Gruet, O. Pirali, T. Chamaillé, G. Mouret, *Spectroc. Acta A* **2014**, *132*, 838–845.
[14] A. Cuisset, I. Smirnova, R. Bocquet, F. Hindle, G. Mouret, C. Yang, O. Pirali, P. Roy, A. Predoi-Cross, B. E. Billinghurst, *AIP Proceedings* **2010**, *1214*, 85–87.
[15] M. Cirtog, P. Asselin, P. Soulard, B. Tremblay, B. Madebéne, M. E. Alikhani, R. Georges, A. Moudens, M. Goubet, T. R. Huet, O. Pirali, P. Roy, *J. Phys. Chem. A* **2011**, *115*, 2523–2532.
[16] P. Asselin, J. Bruckhuisen, A. Roucou, M. Goubet, M.-A. Martin-Drumel, A. Jabri, Y. Belkhodja, P. Soulard, R. Georges, A. Cuisset, *J. Chem. Phys.* **2019**, *151*, 194302.
[17] A. Roucou, I. Kleiner, M. Goubet, S. Bteich, G. Mouret, R. Bocquet, F. Hindle, W. L. Meerts, A. Cuisset, *ChemPhysChem* **2018**, *18*, 1056–1067.
[18] J. A. Widegren, T. J. Bruno, *J. Chem. Eng. Data* **2009**, *55*, 159–164.
[19] M. H. Pickett, *J. Mol. Spectrosc.* **1991**, *148*, 371–377.
[20] V. V. Ilyushin, Z. Kisiel, L. Pszczólkowski, H. Mäder, J. T. Hougen, *J. Mol. Spectrosc.* **2010**, *259*, 26–38.
[21] V V. Ilyushin, E. A. Alekseev, Z. Kisiel, L. Pszczółkowski, *J. Mol. Spectrosc.* **2017**, 339, 31–39.
[22] A. Belloche, A. A. Meshcheryakov, R. T. Garrod, V. V. Ilyushin, E. A. Alekseev, R. A. Motiyenko, L. Margulés, H. S. P. Müller, K. M. Menten, *Astron. Astrophys.* **2017**, *601*, A49.
[23] V. V. Ilyushin, *J. Mol. Spectrosc.* **2018**, *345*, 64–69.
[24] Z. Kisiel, E. Białkowska-Jaworska, L. Pszczółkowski, *J. Chem. Phys.* **1998**, *109*, 10263–10272.
[25] Z. Kisiel, E. Białkowska-Jaworska, L. Pszczółkowski, *J. Mol. Spectrosc.* **2000**, *199*, 5–12.
[26] I. Kleiner, *J. Mol. Spectrosc.* **2010**, *260*, 1–18.
[27] R. Kannengießer, W. Stahl, H. V. L. Nguyen, I. Kleiner, *J. Phys. Chem. A* **2016**, *120*, 3992–3997.
[28] H. Hartwig, H. Dreizler, *Z. Naturforsch. A* **1996**, *51*, 923–932.
[29] N. Hansen, H. M"ader, T. Bruhn, *Mol. Phys.* **1999**, *97*, 587–595.
[30] E. L. Hahn, T. P. Das, *Nuclear quadrupole resonance spectroscopy*. New York, Academic Press, **1958**.
[31] W. C. Bailey, *Chem. Phys.* **2000**, *252*, 57–66.
[32] M. H. Palmer, *Z. Naturforsch. A* **1996**, *51a*, 451–459.
[33] A. Jabri, D. Fontanari, A. Roucou, C. Bray, F. Hindle, G. Dhont, G. Mouret, R. Bocquet, A. Cuisset, *J. Chem. Phys.* **2019**, *150*, 104303.
[34] H. Saal, J.-U. Grabow, A. R. Hight Walker, J. T. Hougen, I. Kleiner, W. Caminati, *J. Mol. Spectrosc.* **2018**, *351*, 55–61.
[35] F. Hindle, R. Bocquet, A. Pienkina, A. Cuisset, G. Mouret, *Optica* **2019**, *6*, 1449.
[36] M. A. Koshelev, I. I. Leonov, E. A. Serov, A. I. Chernova, A. A. Balashov, G. M. Bubnov, A. F. Andriyanov, A. P. Shkaev, V. V. Parshin, A. F. Krupnov, M. Y. Tretyakov, *IEEE T. THZ Sci. Techn.* **2018**, *8*, 773–783.
[37] M. Tudorie, L. H. Coudert, T. R. Huet, D. Jegouso, G. Sedes, *J. Chem. Phys.* **2011**, *134*, 074314.
[38] S. Kassi, D. Petitprez, G. Wlodarczak, *J. Mol. Struct.* **2000**, *517*, 375–386.
[39] S. Kassi, D. Petitprez, G. Wlodarczak *J. Mol. Spectrosc.* **2004**, *228*, 293–297.
[40] G. Mouret, M. Guinet, A. Cuisset, L. Croize, S. Eliet, R. Bocquet, F. Hindle, *IEEE Sens. J.* **2013**, *13*, 133–138.
[41] A. Roucou, D. Fontanari, G. Dhont, A. Jabri, C. Bray, G. Mouret, R. Bocquet, A. Cuisset, *ChemPhysChem* **2018**, *19*, 1–8.
[42] M.-A. Martin-Drumel, F. Hindle, G. Mouret, A. Cuisset, J. Cernicharo, *Astrophys. J.* **2015**, *799*, 115.
[43] M. J. Frisch, G. W. Trucks, H. B. Schlegel, G. E. Scuseria, M. A. Robb, J. R. Cheeseman, G. Scalmani, V. Barone, G. A. Petersson, H. Nakatsuji, X. Li, M. Caricato, A. V. Marenich, J. Bloino, B. G. Janesko, R. Gomperts, B. Mennucci, H. P. Hratchian, J. V. Ortiz, A. F. Izmaylov, J. L. Sonnenberg, D. Williams-Young, F. Ding, F. Lipparini, F. Egidi, J. Goings, B. Peng, A. Petrone, T. Henderson, D. Ranasinghe, V. G. Zakrzewski, J. Gao, N. Rega, G. Zheng, W. Liang, M. Hada, M. Ehara, K. Toyota, R. Fukuda, J. Hasegawa, M. Ishida, T. Nakajima, Y. Honda, O. Kitao, H. Nakai, T. Vreven, K. Throssell, J. A. Montgomery Jr., J. E. Peralta, F. Ogliaro, M. J. Bearpark, J. J. Heyd, E. N. Brothers, K. N. Kudin, V. N. Staroverov, T. A. Keith, R. Kobayashi, J. Normand, K. Raghavachari, A. P. Rendell, J. C. Burant, S. S. Iyengar, J. Tomasi, M. Cossi, J. M. Millam, M. Klene, C. Adamo, R. Cammi, J. W. Ochterski, R. L. Martin, K. Morokuma, O. Farkas, J. B. Foresman, D. J. Fox, Gaussian 16 Revision B.01, **2016**. Gaussian Inc. Wallingford CT.
[44] D. E. Woon, T. H. Dunning Jr, *J. Chem. Phys.* **1994**, *101*, 8877–8893.
[45] R. A. Kendall, T. H. Dunning Jr, R. J. Harrison, *J. Chem. Phys.* **1992**, *96*, 6796–6806.
[46] V. Barone, *J. Chem. Phys.* **2005**, *122*, 014108.
[47] M. Biczysko, P. Panek, G. Scalmani, J. Bloino, V. Barone, *J. Chem. Theory Comput.* **2010**, *6*, 2115–2125.
[48] S. Grimme, M. Steinmetz, *Phys. Chem. Chem. Phys.* **2013**, *15*, 16031–16042.
[49] S. Bteich, M. Goubet, R. A. Motiyenko, L. Margules, T. R. Huet, *J. Mol. Spectrosc.* **2018**, *348*, 124–129.
[50] P. Bunker, *Molecular Symmetry and Spectroscopy*. Elsevier, **2012**.
[51] C. C. Lin, J. D. Swalen, *Rev. Mod. Phys.* **1959**, *31*, 841.
[52] A. P. Cox, S. Waring, K. Morgenstern, *Nature Phys. Science* **1971**, *229*, 22–23.
[53] J.-U. Grabow, *Handbook of high-resolution spectroscopy, Vol. 2.* John Wiley & Sons, Ltd, **2011**.
[54] J. T. Hougen, I. Kleiner, M. Godefroid, *J. Mol. Spectrosc.* **1994**, *163*, 559–586.
[55] I. Kleiner, J. T. Hougen, *J. Chem. Phys.* **2003**, *119*, 5505–5509.
[56] D. Gerhard, A. Hellweg, I. Merke, W. Stahl, M. Baudelet, D. Petitprez, G. Wlodarczak, *J. Mol. Spectrosc.* **2003**, *220*, 234–241.
[57] S. Jacobsen, U. Andresen, H. Mader, *Struct. Chem.* **2003**, *14*, 217–225.
[58] R. G. Bird, D. W. Pratt, *J. Mol. Spectrosc.* **2011**, *266*, 81–85.
[59] H. D. Rudolph, K. Walzer, I. Krutzik, *J. Mol. Spectrosc.* **1973**, *47*, 314–339.
[60] A. Welzel, A. Hellweg, I. Merke, W. Stahl, *J. Mol. Spectrosc.* **2002**, *215*, 58–65.
[61] L. Ferres, H. Mouhib, W. Stahl, H. V. L. Nguyen, *ChemPhysChem* **2017**, *18*, 1855–1859.

[62] K. P. Rajappan Nair, S. Herbers, A. Lesarri, J.-U. Grabow, *J. Mol. Spectrosc.* **2019**, *361*, 1–7.
[63] L. D. Stewart, J. R. Gascooke, W. D. Lawrance, *J. Chem. Phys.* **2019**, *150*, 174303.
[64] C. Thomsen, H. Dreizler, *Z. Naturforsch. A* **2001**, *56*, 635–640.
[65] T. Bruhn, H. Mäder, *J. Mol. Spectrosc.* **2000**, *200*, 151–161.
[66] A. Hellweg, C. Haettig, I. Merke, W. Stahl, *J. Chem. Phys.* **2006**, *124*, 204305.
[67] G. Myszkiewicz, W. L. Meerts, C. Ratzer, M. Schmitt, *Phys. Chem. Chem. Phys.* **2005**, *7*, 2142–2150.
[68] A. J. Shirar, D. S. Wilcox, K. M. Hotopp, G. L. Storck, I. Kleiner, B. C. Dian, *J. Phys. Chem. A* **2010**, *114*, 12187–12194.
[69] L. Ferres, W. Stahl, H. V. L. Nguyen, *J. Chem. Phys.* **2018**, *148*, 124304.
[70] G. E. Herberich, *Z. Naturforsch. A* **1967**, *22*, 761–764.
[71] J. Rottstegge, H. Hartwig, H. Dreizler, *J. Mol. Struct.* **1999**, *478*, 37–47.
[72] X.-Q. Tan and D. W. Pratt, *J. Chem. Phys.* **1994**, *100*, 7061–7067.
[73] P. J. Breen, J. A. Warren, E. R. Bernstein, J. I. Seeman, *J. Chem. Phys.* **1987**, *87*, 1917–1926.
[74] M. Fujii, M. Yamauchi, K. Takazawa, M. Ito, *Spectroc. Acta A* **1994**, *50*, 1421–1433.
[75] A. Hellweg, C. Hättig, *J. Chem. Phys.* **2007**, *127*, 024307.
[76] L. Ferres, W. Stahl, I. Kleiner, H. V. L. Nguyen, *J. Mol. Spectrosc.* **2018**, *343*, 44–49.

Manuscript received: July 10, 2020
Revised manuscript received: August 27, 2020
Accepted manuscript online: August 28, 2020
Version of record online: ■■, ■■

ARTICLES

Anisotropic internal rotation coupling revealed in an explosive taggant: The complete study of large amplitude torsions in nitrotoluene isomers by mean of high resolution microwave and mm-wave spectroscopy allowed to provide rotational line lists crucial for explosive taggants detection in gas phase. Quantum chemistry calculations performed on 2-NT has revealed an anisotropic back-and-forth internal rotation of $-CH_3$ and $-NO_2$.

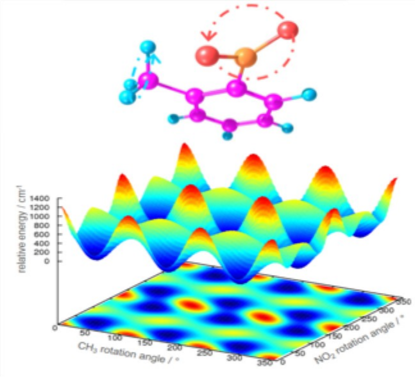

Dr. A. Roucou, Dr. M. Goubet, Prof. I. Kleiner, Dr. S. Bteich, Prof. A. Cuisset**

1 – 17

Large Amplitude Torsions in Nitrotoluene Isomers Studied by Rotational Spectroscopy and Quantum Chemistry Calculations